Mon. Not. R. Astron. Soc. **000**, 1–13 (2013) Printed 4 April 2014 (MN LaTeX style file v2.2)

The effect of starspots on the radii of low-mass pre-main sequence stars

R. J. Jackson and R. D. Jeffries
Astrophysics Group, Research Institute for the Environment, Physical Sciences and Applied Mathematics, Keele University, Keele, Staffordshire ST5 5BG

arXiv:1404.0683v1 [astro-ph.SR] 2 Apr 2014

2nd April 2014, MNRAS in press

ABSTRACT

A polytropic model is used to investigate the effects of dark photospheric spots on the evolution and radii of magnetically active, low-mass ($M < 0.5\,M_{\odot}$), pre-main sequence (PMS) stars. Spots slow the contraction along Hayashi tracks and inflate the radii of PMS stars by a factor of $(1-\beta)^{-N}$ compared to unspotted stars of the same luminosity, where β is the equivalent covering fraction of dark starspots and $N \simeq 0.45 \pm 0.05$. This is a much stronger inflation than predicted by the models of Spruit & Weiss (1986) for main sequence stars with the same β, where $N \sim 0.2$–0.3. These models have been compared to radii determined for very magnetically active K- and M-dwarfs in the young Pleiades and NGC 2516 clusters, and the radii of tidally-locked, low-mass eclipsing binary components. The binary components and ZAMS K-dwarfs have radii inflated by ~ 10 per cent compared to an empirical radius-luminosity relation that is defined by magnetically inactive field dwarfs with interferometrically measured radii; low-mass M-type PMS stars, that are still on their Hayashi tracks, are inflated by up to ~ 40 per cent. If this were attributable to starspots alone, we estimate that an effective spot coverage of $0.35 < \beta < 0.51$ is required. Alternatively, global inhibition of convective flux transport by dynamo-generated fields may play a role. However, we find greater consistency with the starspot models when comparing the loci of active young stars and inactive field stars in colour-magnitude diagrams, particularly for the highly inflated PMS stars, where the large, uniform temperature reduction required in globally inhibited convection models would cause the stars to be much redder than observed.

Key words: stars: rotation – stars: magnetic activity; stars: low-mass – clusters and associations: NGC 2516.

1 INTRODUCTION

There is increasing evidence that the radii of fast rotating, magnetically active K- and M-dwarf stars are inflated relative to the predictions of evolutionary models. Measurements of eclipsing binaries suggest that radii can be 10–15 per cent larger than expected, at a given mass, for binary components with $M < 0.7\,M_{\odot}$ (Lopez-Morales 2007; Morales et al. 2009; Torres 2013). The components of these close binary pairs are expected to be tidally locked and fast-rotating, hosting strong, dynamo-generated magnetic fields. It has been suggested that the relative increase in radius is associated with this magnetic activity (Lopez-Morales 2007), although it is difficult to find slowly rotating, magnetically inactive eclipsing binaries with which to test this hypothesis.

The same comparison between observation and theory cannot easily be made for single stars since a direct measurement of their masses is not possible. However, it is possible to compare the radii and luminosities of nearby field stars with the predictions of evolutionary models. Boyajian et al. (2012b, hereafter BM12) reported the interferometric angular diameters of K- and M-dwarfs with precise Hipparcos parallaxes and used these to determine an empirical radius-luminosity relation for main sequence (MS) stars over the temperature range 3200–5500 K. The radii of these relatively inactive field stars show satisfactory agreement with the predicted radii of evolutionary models for K- and early M-dwarfs (e.g. the BCAH98 model of Baraffe et al. 1998) but for later M-dwarfs (spectral types M2 to M4), models generally underestimate radii (by ~ 8 per cent in the case of the BCAH98 model; ~ 5 per cent for the Dartmouth models of Dotter et al. 2008). No such comparisons have been made for magnetically active stars since there are no very active field M-dwarfs close enough to allow a precise interferometric radius measurement.

Jackson, Jeffries & Maxted (2009) estimated the mean radii for groups of rapidly rotating, highly magnetically active, late K- and M-dwarfs in the young open cluster NGC 2516 (age $\simeq 140$ Myr – Meynet, Mermilliod and Maeder 1993) using the product of their rotation periods and projected equatorial velocities. They found that their mean radii at a given luminosity are larger than model predictions and also larger than the interferometric radii of magnetically inactive dwarfs. The discrepancy rises from ~ 10 per cent for late K-dwarfs to as much as ~ 50 per cent for M4

© 2013 RAS

dwarfs that are nearly or fully convective. This result supports the suggestion that the radius inflation (at a given luminosity) is due to rotationally induced magnetic activity. Further measurements are required to correlate radius inflation with rotation, magnetic field strength and other magnetic activity indicators, but there is sufficient evidence of a causal link to have stimulated theoretical studies. Two mechanisms related to dynamo-generated magnetic fields have been suggested that could inflate the radii of K- and M-dwarfs: inhibition or stabilisation of convection (e.g. Mullan & MacDonald 2001; Chabrier et al. 2007; Feiden & Chaboyer 2012, 2013a,b; MacDonald & Mullan 2013); or the effect of cool, magnetic starspots (Spruit 1982; Spruit & Weiss 1986; Chabrier et al. 2007).

Mullan and MacDonald (2001) modelled the effect of interior magnetic fields by modifying the Schwarzschild criterion and suppressing convection. Chabrier et al. (2007) inhibited the convective efficiency by artificially reducing the convective mixing-length parameter. Feiden & Chaboyer (2012, 2013b) described a modification to the Dartmouth evolutionary code that takes account of the effect of magnetic field on the equation of state and on mixing-length theory. In their papers they give examples that produce the modest (10 per cent) observed radius inflation of the components of several eclipsing binaries of mass $0.4 < M/M_{\odot} < 1.0$, although the predicted surface magnetic fields are a few times higher than observational estimates. This explanation of radius inflation becomes less plausible for lower mass stars where convective heat transfer is more and more efficient. Either much larger changes in effective mixing length are required to produce even a 10 per cent radius inflation in nearly or fully convective stars (e.g. the binary CM Dra), or interior magnetic field strengths would need to approach 50 MG to sufficiently stabilise the star against convection, which are considered too high to be physically plausible (Feiden & Chaboyer 2013a).

An alternative mechanism is the effect of starspots in reducing heat flux out of the photosphere. Spruit & Weiss (1986, hereafter SW86), modelled the effect of starspots on zero age main sequence (ZAMS) stars in the mass range 0.2–1.9 $M_{\odot}$. They argued that the radius, luminosity and temperature of the unspotted surface would adapt on the Kelvin-Helmholtz timescale of the convective envelope to achieve thermal equilibrium. For low-mass stars with deep convective envelopes they used a polytropic model to show that the effect of starspots is to reduce the luminosity of the star at near-constant radius and temperature of the unspotted photosphere, hence lowering the *effective* temperature. For higher mass stars, where the mass of the convective envelope is a small fraction of the stellar mass, SW86 used a numerical model to show that the effect of starspots would be to increase the temperature of the unspotted photosphere while the radius and luminosity are nearly unchanged.

Which of these mechanisms is dominant is undecided and likely to depend on the fraction of the photosphere covered by dark starspots. The presence of starspots on magnetically active stars is a well documented phenomenon. Evidence for dark starspots and their associated magnetic fields came initially from observations of rotational modulation of broadband fluxes (e.g. Hall 1972, Eaton & Hall 1979) but there is now a large literature that detects and investigates starspots using direct and indirect observational techniques such as Doppler imaging (Collier-Cameron & Unruh 1994; Strassmeier 2002), spectroscopy of Zeeman-broadened lines (e.g. Marcy 1982, Johns-Krull & Valenti 1996), and tomography using circularly polarized light (Zeeman Doppler Imaging - Semel 1989, Donati et al. 1997). However, the relevant question here is whether spots cover enough area of the surface to significantly reduce the stellar luminosity? Spot coverage and spot temperatures have been determined for very active G- and K-stars from their optical TiO absorption bands, indicating filling factors of 20–50 per cent, with temperature ratios between spotted and unspotted photosphere of 0.65–0.76 (O'Neal, Neff & Saar 1998; O'Neal et al. 2004; O'Neal 2006). If starspots are present at similar filling factors on active K- and M-dwarfs then this could significantly reduce their luminosity at a given radius.

MacDonald and Mullan (2013) compared measurements of (projected) radii measured on young active M-dwarfs in NGC 2516 (Jackson et al. 2009) with their numerical models that include a prescription for magnetic suppression of convection and cool starspots. They found that, for models in which only the effects of spots are included, the mean radii of the coolest stars in the sample would require a spot coverage of more than 79 per cent of the photosphere. As they considered this implausible they rejected spots as the main cause of radius inflation. Their estimate of the increase in radii was made by comparison to a model for the radii of inactive stars and, as we show in this paper, a significantly lower estimate of filling factor is obtained if the radii of active stars are instead compared to an empirical radius-luminosity relation for inactive main sequence stars (e.g. from BM12).

SW86 estimated the effect of starspots only for ZAMS stars, where the luminosity depends on the temperature of their nuclear burning cores. The cool M-dwarfs in NGC 2516, which show the largest apparent increase in radius relative to inactive stars, are still in their pre-main sequence (PMS) phase. They are likely to be fully convective with luminosity produced chiefly by the release of gravitational energy, and might respond differently to starspots. In this paper we: (a) extend the work of SW86 to include the effect of starspots on low-mass PMS stars; (b) use the recently reported radius-luminosity relation of BM12 for inactive MS stars as a baseline against which to assess the increase in radius of active K- and M- dwarfs; and (c) compare these models with the published radii of eclipsing binaries, and with the radii of highly active K- and M-dwarfs, including a new analysis of the projected radii of stars in the young Pleiades cluster. We find that PMS stars are more inflated for a given level of spot coverage than ZAMS stars of a similar luminosity and that the spot coverage required to produce the measured radii is large but perhaps not excessive. Finally it is shown that, in contrast to models that suppress convective flux and uniformly lower the photospheric temperature, the spot model is able to simultaneously match the loci of very active stars in colour-magnitude diagrams.

2 THE RADIUS INFLATION PRODUCED BY STARSPOTS ON LOW-MASS PMS STARS

2.1 A polytropic model of PMS stars

The effect of starspots on the radius, luminosity, and temperature of PMS stars is determined using a polytropic model of the star in the Hayashi zone (Prialnik 2000). Taking the simplest of the formulations given by SW86, where the effect of starspots is solely to inhibit radiation from the photosphere, reducing the luminosity of the star to

$$L = 4\pi\sigma\,(1-\beta)\,R^2\,T^4\,, \qquad (1)$$

where R is the radius , T the temperature of the unspotted photosphere, and σ is Stefan's constant. β is the equivalent filling factor of completely dark starspots that would produce the same luminos-

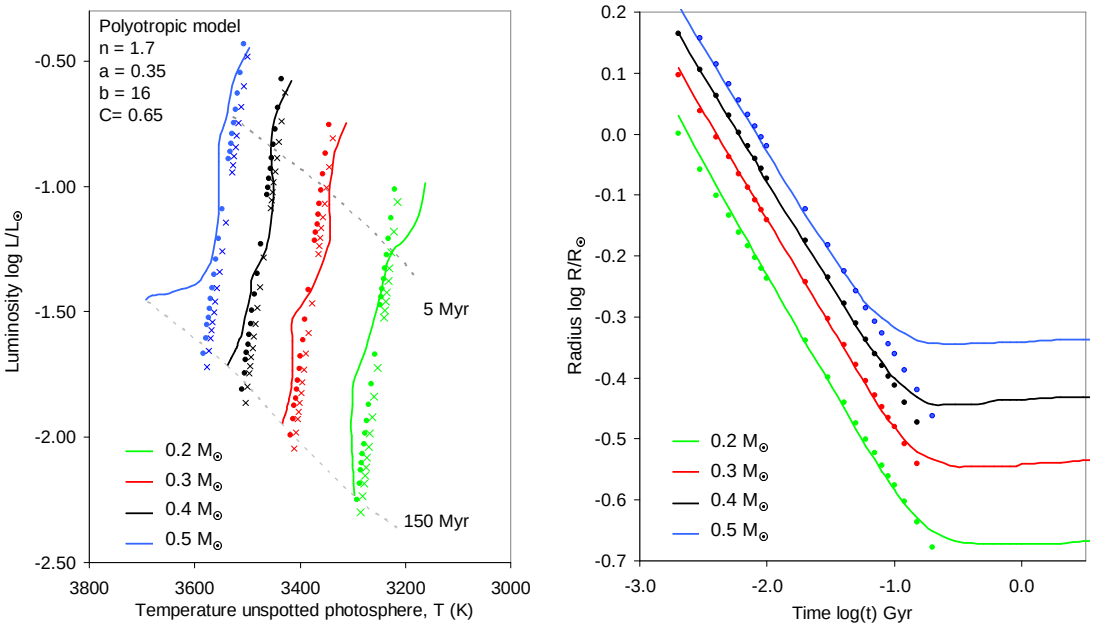

Figure 1. Evolutionary tracks for, 0.2, 0.3, 0.4 and 0.5 solar mass stars over the age range 5 to 150Myr. The solid lines in the left hand plot show evolutionary tracks from the BCAH98 model of stellar evolution ([M/H]=0, Y=0.275, L_{mix} =H_P). The filled circles show the evolutionary tracks predicted using a polytropic model of an unspotted star on the Hayashi track with constants adjusted to match approximately the BCAH98 tracks. The crosses show the effect of 30 percent coverage of dark starspots for the same polytropic model. The right hand plot shows the variation of radius with time. The lines show the BCAH98 model and the filled circles show results of the polyropic model of an unspotted star.

ity reduction as the actual coverage of starspots at the real (non-zero) starspot temperature.

Prialnik (2000, Eqns. 8.11 and 8.13) gives the following relation between the luminosity of an unspotted star, L_u, on the Hayashi track, as a function of T and mass, M.

$$\log L_u = A \log T + B \log M + \text{constant}, \tag{2}$$

where

$$A = \frac{(7-n)(a+1) - 4 - a + b}{(3-n)(a+1)/2 - 1} \text{ and}$$

$$B = -\frac{(n-1)(a+1)+1}{(3-n)(a+1)/2 - 1}.$$

Here, n is the polytropic index and the exponents a and b describe the rate of change of the Rosseland mean opacity as a function of surface density, ρ, and T, as $\kappa = \kappa_0 \rho^a T^b$. Rearranging this expression and reducing the luminosity to represent the effects of starspots (i.e. $L = (1-\beta)\, L_u$) gives the following expression for the luminosity of a spotted polytropic star;

$$\frac{L}{L_\odot} = C^{-A}(1-\beta)\left(\frac{M}{M_\odot}\right)^B \left(\frac{T}{T_\odot}\right)^A, \tag{3}$$

where C is a constant that depends on n, a, b and κ_0.

The luminosity of a star on the Hayashi track results from the release of gravitational energy as its radius contracts. The gravitational potential energy of a polytropic star is given by $\Omega = -\frac{3}{5-n} GM^2/R$ (Hayashi, Hoshi and Sugimoto 1962). Applying the virial theorem gives the luminosity, $L = -\frac{1}{2}\frac{\partial \Omega}{\partial t}$, as a function of time, t;

$$\frac{L}{L_\odot} = -\frac{3}{(10-2n)}\left(\frac{GM_\odot^2}{L_\odot R_\odot}\right)\left(\frac{M}{M_\odot}\right)^2 \left(\frac{R}{R_\odot}\right)^{-2} \frac{\partial (R/R_\odot)}{\partial t}. \tag{4}$$

Eliminating, L and T from Eqns. 2 and 3 gives the rate of change of radius with time as;

$$\frac{d(R/R_\odot)}{dt} = -Z(1-\beta)\left(\frac{4-A}{4-3A}\right)\left(\frac{R}{R_\odot}\right)^{\frac{8-4A}{4-A}} \left(\frac{M}{M_\odot}\right)^{\frac{2A+4B-8}{4-A}}, \tag{5}$$

where the constant

$$Z = \frac{(10-2n)(4-3A)}{3(4-A)}\left(\frac{L_\odot R_\odot}{GM_\odot^2}\right) C^{\frac{-4A}{4-A}}.$$

Integrating this expression and using the boundary condition of infinite radius at zero time gives the radius of an unspotted polytropic star as a function of time;

$$\frac{R}{R_\odot} = (Zt)^{\frac{A-4}{4-3A}} \left(\frac{M}{M_\odot}\right)^{\frac{8-2A-4B}{4-3A}}. \tag{6}$$

If spots with an effective filling factor β develop at a time t_s then the radius at time $t > t_s$ is given by

$$\frac{R}{R_\odot} = [Zt(1-\beta) + Zt_s\beta]^{\frac{A-4}{4-3A}} \left(\frac{M}{M_\odot}\right)^{\frac{8-2A-4B}{4-3A}}, \tag{7}$$

and the resultant luminosity is given by

$$\frac{L}{L_\odot} = (1-\beta) C^{\frac{-4A}{4-A}} [Zt(1-\beta) + Zt_s\beta]^{\frac{2A}{4-3A}} \left(\frac{M}{M_\odot}\right)^{\frac{4B-4A}{4-3A}}. \tag{8}$$

Figure 1 compares the evolutionary tracks and radius as a function of time predicted by the BCAH98 model (for [M/H]=0,

Y=0.275 and $L_{\rm mix}$ =H_P) with the results of the polytropic model for parameter values $A = -132$, $B = 14$ and $n = 1.73$ (corresponding to $a = 0.35$ and $b = 16$ in Eqn. 2). The constants of the polytropic model are set to match the average properties of the BCAH98 model for masses of 0.2, 0.3 and 0.4 $M_{\odot}$ over the age range 20 to 100 Myr. Exponents A and B are scaled to match the slope of radius versus time (Eqn. 7) and the rate of change of T with M (Eqn. 3). Constant C is set to match the average temperature as a function of L in the Hertzsprung-Russell (HR) diagram and n, is chosen to match the average radii as a function of time to the BCAH98 values (Eqn. 7). Constants a and b which scale the mean Rosseland opacity are then found from Eqn. 2.

There is good agreement (see Fig. 1) between this polytropic model and the BCAH98 model for $M \leqslant 0.4\,M_{\odot}$, indicating that these lower mass stars are effectively PMS stars following Hayashi tracks at ages up to ~ 150 Myr. The point where stars diverge from the BCAH98 evolutionary tracks coincides with where they leave the Hayashi track and so the model also works at higher masses, but for a more limited age range; a 0.5 $M_{\odot}$ star leaves the Hayashi track at an age of ∼70 Myr. The parameters a and b defining the Rosseland opacity change significantly with temperature (Alexander and Ferguson 1994), but it is shown in section 2.2 that the predictions made using the polytropic model are insensitive to the adoption of constant values for these parameters provided stars follow near-vertical tracks in the HR diagram (i.e $|A| \gg 1$), which they do as long as they remain on Hayashi tracks.

2.2 The effects of starspots on the radius and luminosity of pre-main sequence stars

The polytropic model can be used to predict the effects of starspots on the radius, luminosity and temperature of PMS stars. Figure 2 shows the effects of an intentionally unrealistic case where dark starspots *suddenly* develop at a time $t_s = 10$ Myr to cover 30 per cent (β=0.3) of the surface of a 0.3 $M_{\odot}$ star. The immediate effect is to reduce L by 30 per cent with no change in R or T. The effect of spots is then to slow the subsequent rate of descent along the Hayashi track by a factor $(1-\beta)$. As the star contracts, R follows Eqn. 7, and L follows Eqn. 8 such that after ~ 1 dex in $\log t$, R approaches the limiting radius of a star with β=0.3 and $t \gg t_s$ (Eqn. 6), and the luminosity converges towards its limiting value for $t \gg t_s$. The short term effect of an immediate reduction in luminosity is the same as that described by SW86 for spots on low-mass MS stars with deep convective envelopes; a reduction in L with no change in R and T. However, the longer term behaviour is different; spotted PMS stars show an increase in R relative to an unspotted star and a reduction in L of equal proportion (see below) with only a minimal change in T.

The polytropic model provides simple relationships for the increase in R and reduction in L of spotted stars on the Hayashi tracks when the age of the star is much greater than the age when starspots developed. The limiting values of R and L for $t \gg t_s$ in Eqns. 7 and 8 can be used to compare the luminosity and radius of a spotted star (suffix s), with filling factor β, to those of an unspotted star (suffix u) of the same mass and age;

$$(L_s/L_u)_{M,\,t} = (1-\beta)^{D} \text{ and } (R_s/R_u)_{M,\,t} = (1-\beta)^{-D}, \quad (9)$$

where $D = (A-4)/(3A-4)$.

For large A the exponent D tends to $1/3$. Hence the effect of starspots is to reduce the luminosity of the star while increasing its radius as the $\sim 1/3$ power of the area of unspotted photosphere. Since the mass of single stars cannot be measured directly it is more useful to estimate the effect of starspots on R and T at a fixed L and t. In this case the ratios of R and T for spotted and unspotted stars are;

$$(R_s/R_u)_{L,\,t} = (1-\beta)^{-N} \text{ and } (\mathrm{T_s}/\mathrm{T_u})_{\mathrm{L,\,t}} = (1-\beta)^{-(1/4-\mathrm{N}/2)}, \quad (10)$$

where $N = (A-4)/(2A-2B)$. Note that the temperatures here refer to the *unspotted* part of the photosphere and, for the spotted star, this is *not* the effective temperature.

The exponents in these expressions are constant for a given polytropic model, depending primarily on A, the slope of the evolutionary tracks in the HR diagram. Thus, if the starspots were formed at a sufficiently earlier time ($t \gg t_s$), then the relative change in radius is independent of luminosity whilst the star remains on the Hayashi track.

Figure 3 shows the increase in R and T as a function of β for $N = 0.47$, calculated using the values of A and B that provided the best fit to the BCAH98 model in Section 2.1, which themselves depend on a and b and which are probably dependent on T. To assess the sensitivity of N to changes in the parameters defining the polytropic model, values of a and b were instead determined from the tables of low temperature opacities (at X=0.70 and Z=0.02) of Alexander and Ferguson (1994) for $3160 \leqslant T \leqslant 4000$ K and $0.001 \leqslant \rho \leqslant 0.004\,\mathrm{kg\,m^{-3}}$, representative of the photospheric properties of stars of mass $0.2 < M/M_{\odot} < 0.5$ and ages 10–150 Myr (Siess, Dufour & Forestini 2000). This yields a range of values $0.23 < a < 0.53$ and $2.4 < b < 7.2$, resulting in an exponent N increasing from 0.38 for the youngest, lowest mass stars to 0.45 for the older stars (for a polytropic index $1.5 < n < 2.0$). Fig. 3 shows the relative increase in R and T as a function of β eval-

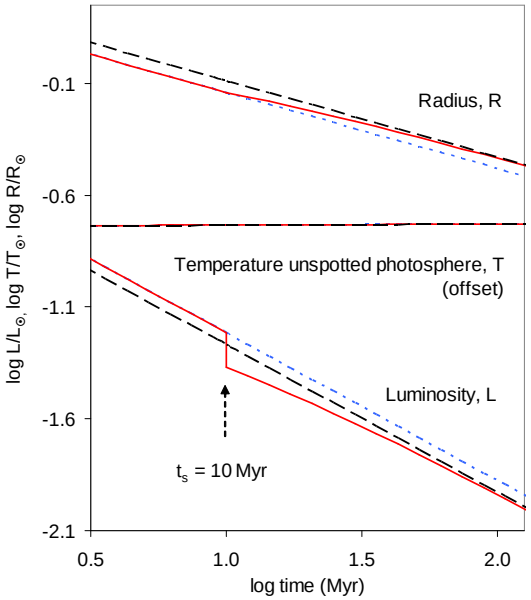

Figure 2. The predicted effects of the sudden inception of 30 per cent coverage by dark starspots on the luminosity, radius and temperature of a PMS star. The lower set of curves show the luminosity as a function of time. The dotted curve shows the track of an unspotted star, the solid line shows the effect of spots developing at an age $t_s = 10$ Myr. The dashed line shows the limiting effect of spot coverage developing much earlier in time ($t \gg t_s$). The central set of curves shows the equivalent changes in the temperature of the unspotted photosphere (which are offset by -0.5 for clarity). The upper curve shows the corresponding changes in radius.

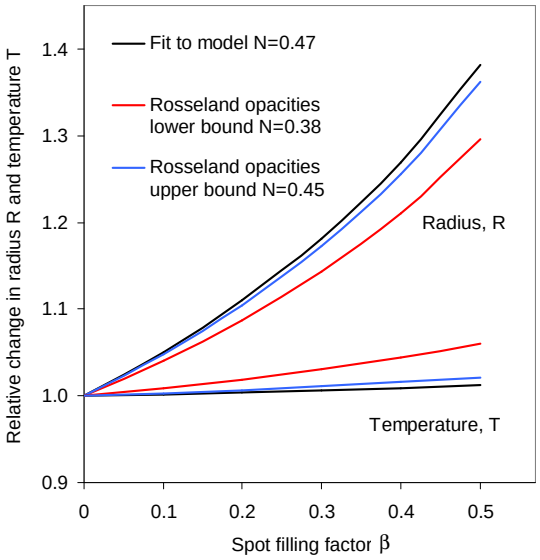

Figure 3. Variation in radius, R and temperature of the unspotted photosphere, T for PMS stars as a function of spot filling factor, compared to an unspotted star of equivalent age and luminosity. Results are shown for different values of polytropic index, n and parameters a and b defining the Rosseland mean opacity ($\kappa = \kappa_0 \rho^a T^b$). The first set shows parameters a, b and n that give the best fit to the BCAH98 evolutionary model (see Fig. 1). The remaining curves show the upper and lower bounds calculated for a practical range of parameter values (see section 2.2).

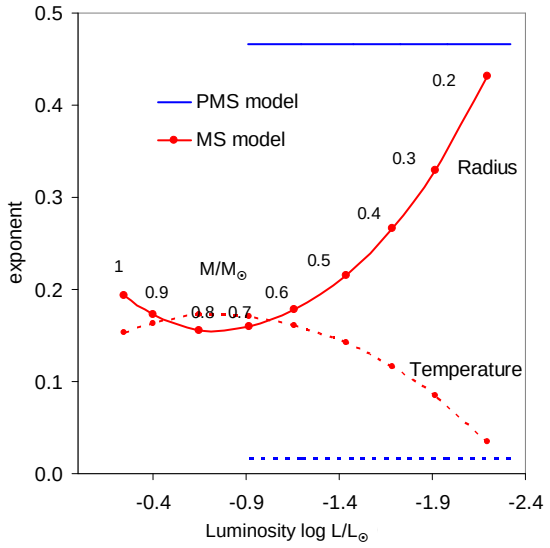

Figure 4. Variation of the exponent N, which determines the increase in radius, R as a function of filling factor of dark starspots, β for stars of fixed age and luminosity ($R_s/R_u \propto (1-\beta)^N$). The curve for MS stars is derived from the results of SW86. The horizontal line for PMS stars shows the result for a polytropic model of stars on the Hayashi track (see Section 2.2). Filled circles on the MS curve indicate model-dependent masses of an unspotted star (from BCAH98). The corresponding temperature exponent, $1/2 - N/4$ gives the increase in temperature of the unspotted part of the photosphere ($T_s/T_u \propto (1-\beta)^{1/2-N/4}$, shown as dashed lines).

uated using these upper and lower bounds for N. These are quite similar to the best fit, indicating that for a practical range of input parameters (n, a and b), the prediction of the polytropic model is that starspots will principally increase the radius of a PMS star (at a given luminosity and age) with a much lower relative increase in temperature, (the index $(1/4 - N/2) < 0.06$). In the limit, as $\partial L/\partial T$ tends to infinity , N tends to 0.5 (see Eqn. 10), in which case R increases with spot coverage as $R_s/R_u = (1-\beta)^{-1/2}$ and T is unchanged.

2.3 The effects of starspots on the radius and luminosity of main sequence stars

Figure 4 shows the variation of the exponent N with luminosity for MS stars using the results of SW86. Figure 8 of SW86 shows the rate of change of L, R and T with β for stars of mass $0.2 < M/M_\odot < 1.9$. For the lowest mass stars the effect of spots is to reduce L with only small increases in R and T. As the stellar mass increases, the reduction in L falls to zero and instead R and T increase with β. Above $\sim 0.8 M_\odot$ the depth of the convective envelope becomes comparable with the predicted depth of inhibited convection below the starspot producing a more complex pattern of changes in L, R and T. SW86 showed that for a $1 M_\odot$ star, the changes in R and T scaled almost linearly with filling factor for $\beta \leqslant 0.12$. In our paper the radii of spotted MS stars at fixed luminosity are scaled as $(1-\beta)^{-N}$ and are extrapolated to higher filling factors than were quoted by SW86. Figure 4 indicates that MS stars show markedly different changes in R and T with β compared to PMS stars on the Hayashi track. The exponent N determining the increase in radius in PMS stars is significantly larger and is independent of luminosity. A principle result of this paper is that a given spot coverage increases the radius (at fixed luminosity) by far more for PMS stars than for MS stars.

3 EMPIRICAL RADIUS-LUMINOSITY RELATIONS FOR K- AND EARLY M-DWARFS

In this section we compare the measured radii of stars from three sources:

- Interferometric radii measured for relatively inactive field stars. These provide a model-independent baseline for comparison with fast-rotating, active stars.
- The average projected radii of fast rotating (projected equatorial velocities, $v \sin i > 8$ km/s), and therefore magnetically active, low-mass stars in two young clusters, NGC 2516 and the Pleiades aged 100–150 Myr (Meynet et al. 1993).
- The radii of short period, magnetically active, eclipsing binary components with known parallaxes and hence calculable luminosities.

Radii are compared as a function of luminosity since there is no model-independent method of measuring the mass of individual stars.

3.1 The radius-luminosity relation of inactive field stars

BM12 used the interferometric radii of 33 MS K- and M-dwarfs to derive an empirical relation for luminosity as a cubic polynomial of radius over the range $-2.8 < \log(L/L_\odot) < -0.3$. Figure 5 shows the resultant radius-luminosity relation together with the measured radii of the field stars. Also shown as open circles are the radii of higher mass stars from Boyajian et al.(2012a) not included in the

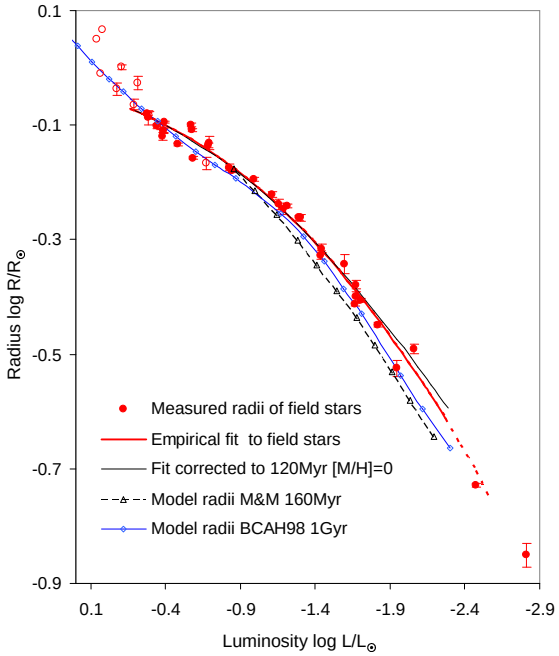
Radius log R/R⊙
Luminosity log L/L⊙
Measured radii of field stars
Empirical fit to field stars
Fit corrected to 120Myr [M/H]=0
Model radii M&M 160Myr
Model radii BCAH98 1Gyr

Figure 5. The radius of unspotted K- and M- dwarfs as a function of luminosity. Filled circles show measured radii from Boyajian et al. 2012b used to define the empirical radius-luminosity relation (thick red line). Open circles show measured data for G stars from Boyajian et al. 2012a. The upper curve (thin black line) shows the empirical radius-luminosity relation "corrected" to 120 Myr and [M/H]=0 as described in section 3.1. The lower curves show a 1 Gyr model isochrone from BCAH98 ([M/H]=0, Y=0.282, L_{mix}=1.9 H_P) and the 160 Myr isochrone used by MacDonald & Mullan (2013) as their "inactive" baseline (see section 3.1).

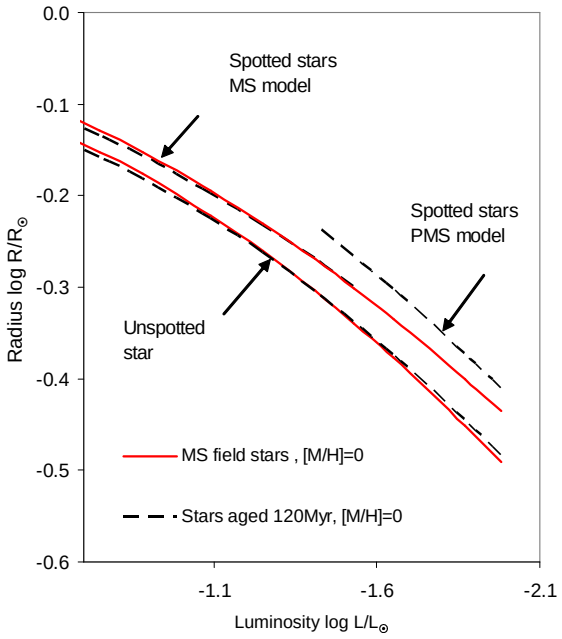

Figure 6. The effect of dark starspots on the radius-luminosity relation of low mass stars. The solid curves show (a) the empirical radius-luminosity relation we adopt for magnetically inactive, solar metallicity, MS field stars (the lower curve) and (b) this curve modified for the effects of 30 per cent coverage by dark starspots, as predicted using the MS model (upper curve). The dashed lines show (a) the empirical relation for magnetically inactive stars corrected to an age of 120 Myr (the lower curve, almost indistinguishable from the inactive field star locus) and (b) the predicted effects of 30 per cent coverage of dark starspots using the MS model for higher luminosity (mass) stars that have left the Hayashi track at 120 Myr (middle curve, almost indistinguishable from the spotted field star curve) and (c) the effects of 30 per cent spot coverage according to the PMS model, appropriate for lower luminosity (mass) stars on their Hayashi tracks (upper curve).

fit. The mean metallicity of the sample stars is [M/H]$= -0.15 \pm 0.21$ and all show relatively low levels of X-ray activity; all but one have $\log(L_x/L_{\rm bol}) < -4.5$ with the highest being -3.5 (BM12), substantially below the "saturated" level of $\log(L_x/L_{\rm bol}) = -3$ seen in the most magnetically active stars (Pizzolato et al. 2003). In this paper the empirical relation of BM12 is assumed to represent magnetically inactive MS stars with [M/H]$= -0.15$.

In order to compare results with radii measured in the Pleiades and NGC 2516 (see Section 3.2), small corrections are added to the empirical relation of BM12 to account for differences in the metallicity and age of these clusters from the field star sample. Soderblom et al. (2009) gives a metallicity of [Fe/H] = $0.03^{+0.02}_{-.05}$ for the Pleiades and Terndrup et al. (2002) gives [Fe/H] = -0.05±0.14 for NGC 2516; i.e. both clusters have near-solar metallicity. The radius-luminosity relation of BM12 shows no obvious dependence on metallicity defined by a sample which has metallicities in the range -0.8 <[Fe/H]< 0.4 . Any dependence is small compared to the uncertainties in luminosity and/or radius over this metallicity range. Nevertheless, the residuals to their polynomial fit do show a weak correlation with metallicity (a Pearson's r coefficient of 0.3). Fitting a regression line to these residuals gives a small correction term such that $\Delta\log(L/L_\odot) = -0.11$([Fe/H]$-0.15$) at fixed R. i.e. $\Delta\log(L/L_\odot) = 0.02$ for a solar metallicity cluster. To take account of the age difference a second correction, $\Delta\log(R/R_\odot)$, is found from the difference between the radius as a function of luminosity predicted at the cluster age and the radius predicted for ZAMS stars (age 1 Gyr) in the BCAH98 models. Results are shown in Fig. 5, where the uppermost curve shows the empirical radius-luminosity relation "corrected" to solar metallicity and an age of 120 Myr. There is a small increase in radius at low luminosities (up to 7 per cent) but a negligible change from the uncorrected BM12 empirical relation if $\log L/L_\odot > -1.5$.

Comparing the empirical radius-luminosity curve in Fig. 5 with the 1 Gyr, [M/H]=0.0 isochrone of BCAH98 shows an increasing discrepancy at low luminosities ($\log L/L_\odot < -1.5$) where the empirical fit is ~ 8 per cent above the BCAH98 model after accounting for the metallicity difference. This is a significant difference. The scatter of measured radii around the empirical relationship is about 6 per cent (see fig.12 of BM12) for low mass stars, leading to a systematic uncertainty of 2–3 per cent in its definition at low luminosities. The lowest curve in Fig. 5 shows the baseline radii used by MacDonald and Mullan (2013) to represent stars in NGC 2516 with no magnetically induced increase in radius. At low luminosities ($-2.3 < L/L_\odot < -1.5$) these radii are about 15 per cent less than the empirical relation of BM12 (corrected to [M/H]=0, 120 Myr). This difference cannot be accounted for by age uncertainties for the cluster. The adoption of such a different zero-activity baseline will of course lead to corresponding differences in the inferred radius inflation and hence the levels of starspot coverage required to explain the observed radii of active stars.

The (corrected) empirical radius-luminosity curve in Fig. 5 can now be scaled using Eqn. 9 and the exponent values shown in

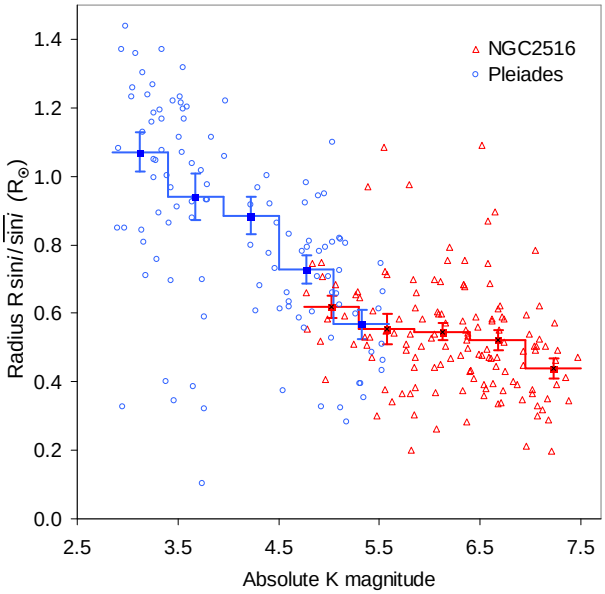

Figure 7. The mean radii of K- and M-dwarfs in NGC 2516 and the Pleiades. Points show the projected radii of individual targets normalised to the mean $\sin i$ ($R \sin i / R_{\odot} \overline{\sin i}$). Solid lines show the average radius measured in 5 equal bins for each cluster (see Table 2).

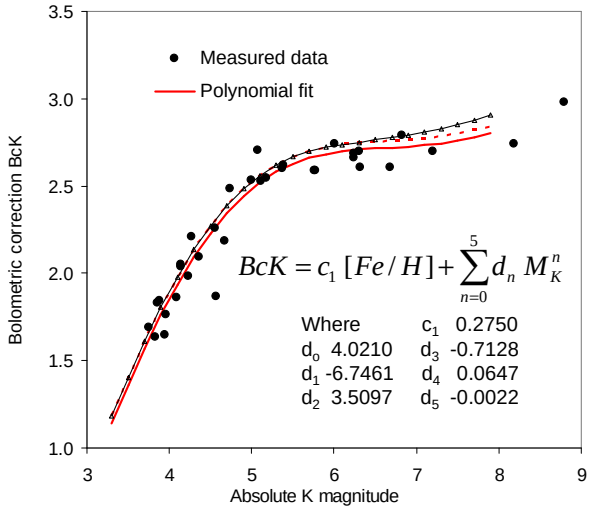

Figure 8. The bolometric correction of K- and M-dwarf stars with measured radii as a function of their absolute K magnitude. Filled circles show the fitted data points from Table 7 and 8 of BM12. The coefficients c_1 and d_n give the polynomial fit to the measured data over the range $3.3 < M_K < 8.0$. The solid and dotted lines shows the polynomial evaluated at the mean metallicity of [M/H]$= -0.15$ and [M/H]$= 0$ respectively. The solid line marked with small triangles shows the bolometric correction corrected to an age of 120 Myr and [M/H]$= 0$ as described in section 3.2.

Fig. 4 to predict the effects of spot coverage on PMS and MS stars. Typical results are shown in Fig. 6 for low mass stars of luminosity $-0.7 > \log L/L_{\odot} > -2.0$. The solid lines shows the radius-luminosity relation for inactive ZAMS stars and the predicted radius inflation due to the effect of 30 per cent coverage ($\beta = 0.3$) of dark starspots *on a MS star*. Also shown as dashed lines are results for stars aged 120 Myr. At this age the higher luminosity (and mass) stars, with $\log L/L_{\odot} \geqslant -1.3$, are expected to be approaching the MS and lower luminosity stars to be PMS. For unspotted stars and for spotted stars on the MS the change in age produces only a small ($<$0.01 dex) increase in $\log R$ relative to the ZAMS. However, the effect of the same starspot coverage on the low-mass PMS stars is predicted to be much larger (by a factor of two) than the ZAMS stars. Hence the radius inflation as a function of luminosity and age will depend on whether stars are best represented by MS or PMS models (see section 4).

3.2 The radii of highly active stars in NGC 2516 and the Pleiades

The radii of low mass stars in NGC 2516 and the Pleiades are estimated from the rotational period and $v \sin i$ following the method described in Jeffries (2007) and Jackson et al. (2009). The product of these quantities gives the projected radius using the formula $R \sin i / R_{\odot} = 0.02\, P\, v \sin i$, where P is the period in days and $v \sin i$ is in km s^{-1}. Assuming stellar spin axes are randomly oriented (e.g. Jackson & Jeffries 2010a), then the mean value of $R \sin i$ for a group of similar stars can be divided by the average value of $\sin i$ to give an estimate of the mean radius. A complication is that if i were small then it would not have been possible to measure the periods of stars or resolve their $v \sin i$. To account for this, $\sin i$ is averaged over $\tau < i \leqslant \pi/2$, where the cut-off inclination τ is estimated by modelling the distribution of $R \sin i$ values about the mean $R \sin i$ as a function of M_K. Further details are given in Jackson et al. (2009) and this correction turns out to be small (see below).

Data for the Pleiades were taken from Table 1 of Hartman et al. (2010), which reports rotational periods measured from results of the HATNet survey together with $v \sin i$ values from the literature. P, $v \sin i$ and K magnitudes are available for 242 stars. From these we choose a subset of 124 with well-resolved $v \sin i > 8$ km s^{-1}. This limit is imposed to ensure reasonably precise $R \sin i$ values and these stars are also expected to be highly magnetically active (see below). Absolute K magnitudes were calculated using a distance modulus of 5.60$\pm$0.04 estimated from main sequence fitting (Pinsonneault et al. 1998) and a reddening of E(B-V)=0.032 (An, Terndrup & Pinsonneault 2007). Using the relations of Reike & Lebofsky (1985) we estimate $A_K \simeq 0.01$. $R \sin i$ values were averaged in 5 equal bins of absolute K magnitude between $2.85 < M_K < 5.60$. The lower cut-off in $\sin i$ was estimated as $\tau = 0.26 \pm 0.10$ radians which yields a mean value of $\sin i = 0.81 \pm 0.02$ (compared to a value of $\pi/4 = 0.79$ if there were no cut-off). Figure 7 shows the estimated radii for individual targets ($R \sin i / \overline{\sin i}$) together with the mean radii in each M_K bin. Uncertainties in the mean are calculated from the measured uncertainties in the mean and the uncertainty in $\overline{\sin i}$ added in quadrature.

Data for low mass stars in NGC 2516 were taken from Table 2 of Jackson and Jeffries (2010b). 141 targets were selected with tabulated values of P, $v \sin i$ and K magnitude and with both $v \sin i > 8$ km s^{-1} and greater than twice its estimated uncertainty. Absolute K magnitudes were calculated using a distance modulus of 7.93$\pm$0.14 from main sequence fitting and a reddening of $E(B-V) = 0.12 \pm 0.02$ (Terndrup et al. 2002), giving $A_K = 0.045$. $R \sin i$ values were averaged in 5 equal bins between $4.75 < M_K < 7.5$. Two targets showing an anomalously large $R \sin i$ (1.5 $R_{\odot}$ and 4.0 $R_{\odot}$) were rejected. The lower cut-off in inclination was estimated as τ=0.40$\pm$0.08 radians, giving $\overline{\sin i} = 0.83 \pm 0.02$. Estimated radii for individual targets are

Table 1. The mean radii of K- and M-dwarfs in NCG 2516 and the Pleiades. The average radii ($\overline{R \sin i}/\overline{\sin i}$) are calculated in 5 equal bins of K magnitude for each cluster. Also shown are the number of targets averaged in each bin, the luminosity calculated from the average absolute K magnitude (using the polynomial fit of BC_K shown in Fig. 8) and the median Rossy number, $\log N_R$.

Cluster	M_K	$\log L/L_\odot$	No.	$R/R_\odot$	$\log N_R$
Pleiades	3.17	0.26+/-0.03	30	1.07+/-0.06	-0.6
Pleiades	3.7	-0.2+/-0.03	29	0.94+/-0.07	-0.6
Pleiades	4.23	-0.62+/-0.03	12	0.89+/-0.05	-1.8
Pleiades	4.78	-0.98+/-0.03	25	0.73+/-0.04	-1.7
Pleiades	5.27	-1.28+/-0.03	19	0.57+/-0.04	-1.9
NGC 2516	5.09	-1.12+/-0.06	13	0.62+/-0.03	-1.7
NGC 2516	5.57	-1.40+/-0.06	26	0.55+/-0.04	-1.9
NGC 2516	6.13	-1.64+/-0.06	36	0.55+/-0.03	-1.9
NGC 2516	6.65	-1.88+/-0.06	37	0.52+/-0.03	-2.2
NGC 2516	7.12	-2.12+/-0.06	25	0.44+/-0.03	-2.4

shown in Fig. 7 together with mean values for each bin. Where the range of luminosities sampled for the two clusters overlaps ($4.7 < M_K < 5.7$), the mean radii agree within their uncertainties.

To assess the likely levels of magnetic activity in these samples, Rossby numbers were calculated from the ratio of period to an empirically estimated convective turnover time. This was calculated such that coronal and chromospheric activity indicators satisfy a single scaling law with Rossby number, independent of stellar mass (e.g. Noyes et al. 1984). We follow the formulation of Pizzolato et al. (2003), setting the turnover time to be $10^{1.1}\,(L/L_\odot)^{-1/2}$ days. The results show that all the target stars in NGC 2516, and all Pleiades stars with $v \sin i$ >8 km/s and $\log L/L_\odot < -0.3$, have $\log N_R < -1$ and are therefore expected to have saturated levels of magnetic activity (Pizzolato et al. 2003; Jackson et al. 2010b; Jeffries et al. 2011). Median values of Rossby number for each of the 5 luminosity bins in each sample are given in Table 1.

To compare the radii of cluster stars with the radii of MS field stars, luminosities are estimated from absolute K magnitudes. BM12 give luminosity as a function of various colours but not absolute magnitude. The luminosities, K magnitudes and distances reported in Tables 7 and 8 of BM12 are used here to fit a polynomial describing the bolometric correction, BC_K against M_K over the range $3.7 < M_K < 8.0$ (see Fig. 8). The Johnson K magnitudes in BM12 are transformed to the CIT system using the conversion giving in Leggett (1992). Once again it is necessary to make a small correction (<0.07 mag.) to account for the younger age and higher metallicity of the clusters compared to the field stars. This correction is determined by comparing the values of BC_K predicted using BT-Settl model atmospheres (Allard et al. 2003) at the cluster age to those at 1 Gyr. The results are shown in Fig. 8 for an age of 120 Myr.

3.3 Potential systematic errors in the projected radii

Hartman et al. (2010) discussed two reasons why there might be systematic errors in the radii estimated from the mean value of $P\,v \sin i$. The first is differential rotation which may cause the rate of surface rotation to reduce towards the poles (Krause & Raedler 1980). Using a solar-type differential rotation law, the rate of differential rotation $\Omega = \Omega_{\rm eq} - \Delta\Omega \sin^2 \Phi$, where $\Omega_{\rm eq}$ is the rate of rotation at the equator, $\Delta\Omega$ is the maximum differential rotation and Φ is the stellar latitude. Assuming starspots are uniformly distributed then the average measured rate of rotation will be $\Omega_m = \Omega_{\rm eq}(1 - \frac{1}{3}\Delta\Omega)$, so the measured period will be a factor $(1 - \frac{1}{3}\Delta\Omega/\Omega_{\rm eq})^{-1}$ greater than the true equatorial period. In the present case the effect of differential rotation is minimised by restricting the sample to relatively fast rotating stars ($v \sin i > 8$ km/s) giving a median angular velocity of 6 radians d^{-1} for NGC 2516 and 3 radians d^{-1} for the Pleiades, compared to a typical differential rotation of $\Delta\Omega \sim 0.07$ radians d^{-1} estimated for active K- and M-dwarfs by Reinhold, Reiners & Basri (2013). Accounting for this level of differential rotation would increase the measured period by < 1 per cent over the true equatorial value, but this would be offset by a small reduction in the measured $v \sin i$ below its true equatorial value. The net change in inferred radius (< 0.3 per cent) is negligible compared to the observed radius inflation and other sources of error.

A second source of error considered by Hartman et al. (2010) is over-estimation of $v \sin i$ from the rotational broadening of spectral lines, due to an under-estimate of the "zero velocity" line widths of reference, slowly rotating stars. This possibility can be tested by restricting the NGC 2516 and Pleiades samples to higher $v \sin i$ objects which are less sensitive to this zero-point error. Increasing the $v \sin i$ threshold to 16 km s^{-1} in NGC 2516 reduces the sample size by 20 per cent and reduces the inferred mean radii by just 1 per cent, which is within the measurement uncertainty. The Pleiades data, containing stars of higher mass, cannot be tested in the same way since there are too few fast-rotating targets with $v \sin i > 16$ km s^{-1}.

3.4 The radii of eclipsing binary stars with known distances

A further source of measured radii as a function of luminosity are eclipsing binary stars of known distance. Table 2 lists the parameters of six binary stars with Hipparcos parallaxes and low-mass components with luminosities in the range $-0.3 > \log(L/L_\odot) > -2.5$. In these cases radii are determined precisely from the eclipse light curves. The temperature ratios are less precise, usually being inferred from spectral type estimates. The total luminosity is calculated from 2MASS K magnitudes transformed to the CIT system (Carpenter 2001) and using the BC$_K$ in Fig. 8 (assuming a metallicity, [Fe/H] $= -0.15$). The K magnitude of a binary is partitioned such that the luminosity of individual components (a and b) is split according to their radii and temperatures (i.e. as $R_a^2 T_a^4 / R_b^2 T_b^4$). The uncertainty in luminosity is calculated from the uncertainty in parallax and the uncertainty in BC$_K$ summed in quadrature. There will be additional systematic errors if the actual metallicity of these stars differs significantly from the mean field star value used to calculate BC$_K$.

4 COMPARING MEASURED AND PREDICTED RADII

The measured radii in Tables 1 and 2 can be compared to the predicted radii of spotted stars as a function of luminosity using the MS and PMS models shown in Fig. 4. To do this it is necessary to decide which model is appropriate for which data i.e. at what luminosity do stars in the Pleiades and NGC 2516 show a radius inflation characteristic of PMS stars, of MS stars, or somewhere in between? This requires estimates of the cluster ages and reference to an evolutionary model. The Pleiades has an age of 100±20 Myr based on nuclear turn off time (Meynet et al. 1993) and an age of 125+/-8 Myr based on the "lithium depletion boundary" (Stauffer

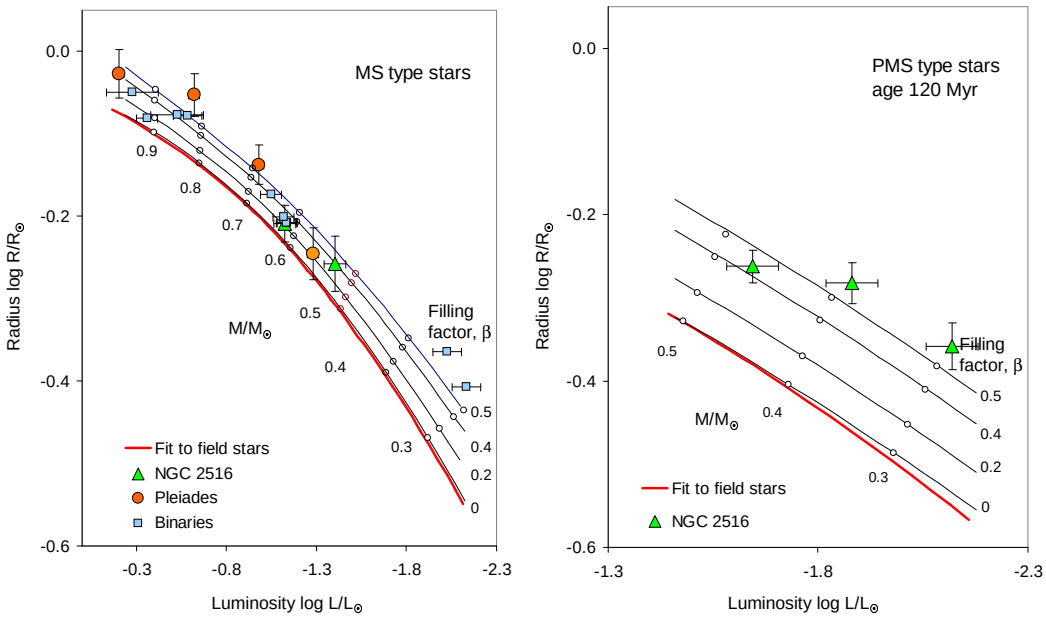

Figure 9. Comparison of the measured radii of fast rotating low mass stars with the predicted radii of MS and PMS stars for different levels of starspot coverage. In the left hand panel the red solid line shows an empirical (magnetically inactive) ZAMS locus (corrected to [M/H]$=0$, see section 3.1). Above this are curves showing the effects of a 20, 40 and 50 per cent coverage by dark starspots (i.e. $\beta = 0.2, 0.4, 0.5$). The right hand panel shows similar curves for PMS stars at an age of 120 Myr. In both plots circles and triangles show the mean radii measured for low-mass stars in NGC 2516 and the Pleiades respectively (see section 3.2); squares show the radii of eclipsing binaries with Hipparcos distances (see section 3.4). The curves are marked at intervals with model-dependent masses (in $M_{\odot}$) from BCAH98.

Table 2. The radii and luminosities of binary star components. Luminosities are calculated from the 2MASS K magnitude (Cutri 2003) and Hipparcos parallaxes (van Leeuwen 2007) as described in section 3.4. Masses, radii and temperature ratios are from Torres, Andersen and Gimenez (2010) except for AE For where data are from Rozyczka el al. (2013).

Identifier	CG Cyg	YY Gem	CU Cnc	UV Psc	V 636 Cen	AE For
$M_a/M_{\odot}$	0.941 +/- 0.014	0.599 +/- 0.005	0.435 +/- 0.001	0.983 +/- 0.008	1.052 +/- 0.008	0.631 +/- 0.004
$M_b/M_{\odot}$	0.814 +/- 0.013	0.599 +/- 0.005	0.399 +/- 0.001	0.764 +/- 0.005	0.855 +/- 0.003	0.620 +/- 0.003
$R_a/R_{\odot}$	0.893 +/- 0.012	0.619 +/- 0.006	0.432 +/- 0.006	1.110 +/- 0.023	1.019 +/- 0.004	0.67 +/- 0.03
$R_b/R_{\odot}$	0.838 +/- 0.011	0.619 +/- 0.006	0.392 +/- 0.009	0.835 +/- 0.018	0.830 +/- 0.004	0.63 +/- 0.03
T_a/T_b	1.114 +/- 0.041	1.000 +/- 0.037	1.011 +/- 0.068	1.217 +/- 0.029	1.180 +/- 0.029	1.011
Parallax (mas)	12.0 +/- 2.2	64.1 +/- 3.8	90.4 +/- 8.2	14.6 +/- 1.3	13.9 +/- 0.9	31.8 +/- 2.0
$K_{\rm 2MASS}$	7.75 +/- 0.02	5.24 +/- 0.02	6.60 +/- 0.02	7.13 +/- 0.02	7.06 +/- 0.02	6.66 +/- 0.02
$\log L_a/L_{\odot}$	-0.28 +/- 0.15	-1.14 +/- 0.06	-2.03 +/- 0.08	0.00 +/- 0.08	0.11 +/- 0.06	-1.05 +/- 0.06
$\log L_b/L_{\odot}$	-0.53 +/- 0.15	-1.14 +/- 0.06	-2.13 +/- 0.08	-0.58 +/- 0.08	-0.36 +/- 0.06	-1.12 +/- 0.06

el al. 1998). NGC 2516 appears to be slightly older; Meynet et al. (1993) gives an age of 140±40 Myr. A mean age of 120±20 Myr is considered representative of both clusters for the present purposes.

One way of splitting the data in Table 1 between the PMS and MS models is to consider the rate of change of radius with time predicted by the BCAH98 model. PMS stars on Hayashi tracks show a linear decrease in $\log R$ with $\log t$ (see Fig. 1), whereas the radii of stars once on the MS is effectively independent of time. For stars aged ~ 120 Myr the break point between the two regimes occurs at $M \sim 0.4\,M_{\odot}$. A more fundamental approach is to consider the age at which stars produce a significant proportion of their losses by nuclear burning, hence altering their response to starspots, and the time taken for the radius of the star to adapt to this change, represented approximately by the thermal timescale of the envelope, $t_{\rm env}$ at this point, defined as the thermal energy contained in the envelop divided by the luminosity of the star (SW86). Table 3 shows estimates of the age at which 50 per cent of the luminosity is provided by hydrogen burning, $t_{\rm nuc}$, and $t_{\rm env}$ at this age, where $t_{\rm nuc}$ and the depth of the envelope are taken from the models of Siess et al. (2000, for Y=0.277, Z=0.02). and $t_{\rm env}$ is calculated for the simple case of a polytropic star with the equation of star of a perfect gas (i.e. n=1.5). Assuming that the starspot coverage remains roughly constant with time then:

(i) Stars with age $t < t_{\rm nuc}$ are expected to exhibit the higher radius inflation characteristic of PMS stars on their Hayashi tracks.

(ii) Stars with age $t_{\rm nuc} < t < t_{\rm nuc} + t_{\rm env}$ are expected to show intermediate levels of radius inflation, relaxing on a timescale $t_{\rm env}$ from their larger PMS radii towards a smaller inflation factor on the MS.

Table 3. Estimates of the age at which nuclear burning contributes 50 per cent of the luminosity, $t_{\rm nuc}$ (from the evolutionary model of Siess et al. 2000) and the themal timescale of the envelope timescale, $t_{\rm env}$, at this age.

Mass ($M_\odot$)	$t_{\rm nuc}$ (Myr)	$t_{\rm env}$ (Myr)
0.1	376	894
0.2	162	306
0.3	123	238
0.4	104	107
0.5	88	50
0.6	75	24

(iii) Stars with $t > t_{\rm nuc} + t_{\rm env}$ are expected to be best represented by the radius inflation predicted for MS stars.

From this, we suggest that stars of age 120±20 Myr and $M \leqslant 0.5M_\odot$ are expected to show radius inflation characteristic of PMS stars, whereas stars of $M > 0.5M_\odot$ have effectively reached the MS. This split is somewhat imprecise and a little model-dependent, however it highlights the importance of $t_{\rm env}$ in determining the increase in radius of spotted stars as they arrive on the MS. Lower mass stars with deep convective zones should retain the radius inflation characteristic of PMS stars long after the inception of nuclear burning.

In Fig. 9 the measured radii in Table 1 are compared with the predicted radii of stars with $\beta = 0, 0.2, 0.4$ and 0.5 for the MS model (left) and the PMS model (right). The small open circles on these models indicate corresponding masses estimated from the BCAH98 model. Based on these values the mean radii for the two higher luminosity bins of the NGC 2516 sample and all of the Pleiades stars (see Table 1) have luminosities corresponding to $M > 0.5M_\odot$ and are therefore compared to the MS models in the left hand panel. The least luminous three bins in the NGC 2516 sample have $M < 0.5M_\odot$ and are compared to the PMS model. Finally, the radii of the eclipsing binary components are compared to the MS model, as these are assumed to be older stars, with their rapid rotation attributable to tidal locking.

Compared to the relationships defined by inactive field stars the highly active stars in NGC 2516 and the Pleiades show a large radius inflation. As a percentage, this inflation is largest for low-mass NGC 2516 stars still in the PMS regime, but is still significant in the MS regime for stars in NGC 2516, the Pleiades and the MS binary components. Table 4 shows the weighted mean radius inflation, $\overline{(R_s - R_u)/R_u}$, for three groups of stars: binary star components (Table 2), stars of the Pleiades and NGC 2516 with $-0.3 > \log(L/L_\odot) > -1.5$ that are in the MS regime and low-mass PMS stars in NGC 2516 with $-1.5 > \log(L/L_\odot) > -2.3$ (Table 1). Also shown in Table 4 are the weighted mean filling factors of *dark* starspots $\overline{\beta}$ that would be required to produce the measured radius inflation, interpolated from the model loci shown in Fig. 9. The quoted uncertainties in $\overline{\beta}$ take account of both the uncertainty in measured radii and the effect of any uncertainty in the luminosity on the predicted radius of an unspotted star. This comparison shows that if the observed radius inflation is produced *solely* by (dark) starspots then this would require filling factors in the range $0.35 < \beta < 0.51$. The actual spot coverage fraction would be even larger for spots of finite temperature. The feasibility of this hypothesis is discussed in the next section.

5 DISCUSSION

Section 2 described a simple polytropic model of a PMS star with dark starspots covering a fraction β of the stellar surface. The model is applicable to stars on the Hayashi track if:

(i) The stars are fully convective, without a radiative or a degenerate core and their luminosity results principally from the rate of change of gravitational potential energy as the star contracts.

(ii) The effect of starspots is to reduce the mean Rosseland opacity averaged over the surface of the star as, $\overline{\kappa} \propto (1 - \beta)$, where β is the equivalent filling factor of dark starspots that would produce the same reduction in total luminosity as the actual coverage of starspots at the actual starspot temperatures.

(iii) The simple relationships governing the radius inflation and change in temperature at a given luminosity (Eqn. 10) assume that the starspots were formed at a much earlier time. This condition seems likely to be met in clusters like NGC 2516 and the Pleiades, because evidence for starspots (e.g. modulation of light curves) is routinely reported in much younger star forming regions (Herbst & Mundt 2005; Irwin & Bouvier 2009).

The model is therefore restricted to a range of masses and ages which must be determined by reference to an evolutionary model for unspotted stars. In this paper the polytropic model is restricted to stars of mass $0.2 < M/M_\odot < 0.5$ for ages $\leqslant$ 120 Myr.

In sections 3 and 4 the predicted increase in radius at a given luminosity as a function of spot coverage is compared with the measured radii of active K- and early M-dwarfs in NGC 2516 and the Pleiades and with the radii of short-period eclipsing binaries with known distances. In our work we have used the polytropic model to scale an empirical relationship between radius and luminosity determined from inactive (and presumably unspotted) field stars with small corrections for differences in age and metallicity. The use of an empirical relation is important; at low luminosities the empirical radius-luminosity relation shows radii 8 per cent higher than the BCAH98 model isochrones (see Fig. 5). If the radii of active stars were compared directly with these model radii it would lead to the inference of an erroneously high level of radius inflation for the lower mass stars.

As an example, Macdonald & Mullan (2013) rejected starspots as the sole cause of radius inflation in the same sample of NGC 2516 stars, on the basis that the lowest luminosity objects would require an excessive (β =0.79) level of spot coverage *relative to their model* of magnetically inactive stars. However, we showed in Fig. 5 that this model significantly underpredicts the interferometrically measured radii of inactive stars by about 15 per cent. Our lower estimate of the required spot coverage ($\beta = 0.51 \pm 0.04$) arises principally because of our comparison with an empirical radius-luminosity relation. Using the empirical radius-luminosity relation does not avoid all systematic uncertainties. There is a radius uncertainty of 2–3 per cent in the mean baseline empirical relationship that can only be improved by more and better measurements of the interferometric radii of inactive low-mass stars. However, this level of systematic uncertainty is small compared to the radius inflation inferred from the projected radii of very active low-mass stars (see Fig. 9 and Table 4).

The level of spot coverage our model requires to solely account for the inflated radii of active stars is $\beta = 0.35$–0.51. This is a little higher than the effective filling factors, β=0.13–0.41, determined for very active G and K-dwarfs from analysis of their TiO absorption bands by O'Neal (2006) but not significantly so. It is still largely unknown what spot coverage fractions and spot temper-

[t]

Table 4. The mean increase in radius and estimated filling factor for (i) binary stars, (ii) higher luminosity stars in the Pleiades and NGC 2516 and (iii) lower luminosity stars in NGC 2516. Filling factors for the first two groups are estimated using a MS model extrapolated from the results of SW86. The filling factor for the third group are estimated using the PMS model described in Section 2.

Sample	Binary Stars with Hipparcos distance	Pleiades and NGC2516	NGC2516
Luminosity	$-0.3 > \log L/L_\odot > -1.5$	$-0.3 > \log L/L_\odot > -1.5$	$-1.5 > \log L/L_\odot > -2.3$
Model used	MS	MS	PMS
Fractional radius increase, $\Delta R/R$	0.08 +/- 0.01	0.13 +/- 0.03	0.40 +/- 0.04
Filling factor dark spots, β	0.35 +/- 0.03	0.45 +/- 0.07	0.51 +/- 0.04

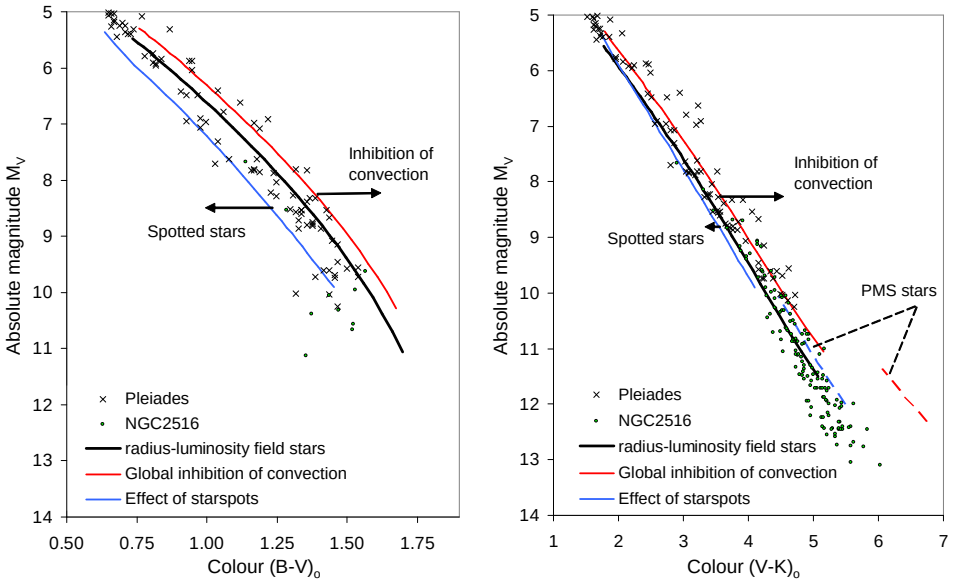

Figure 10. The effect of radius inflation and of starspots on the M_V vs $(B-V)_0$ and M_V vs $(V-K)_0$ CMDs. Points show measured data for highly active stars in NGC 2516 and the Pleiades. The central curves in black shows the empirical radius-luminosity curve for MS field stars corrected to an age of 120 Myr and [M/H]=0. The upper curves in blue show the effects a increase in radius due to magnetic inhibition of convection, 10 percent for MS stars and 30 percent for PMS stars. The lower curves in red show the effects of 50 percent filling factor of starspots with a spot temperature ratio of 0.7 (giving $\beta = 0.4$).

atures might exist on very active M-dwarfs or low-mass PMS stars, though a small value of β seems unlikely given the very high filling factors of kilogauss magnetic field suggested by Zeeman measurements of M dwarfs with $\log N_R < -1$ (Reiners, Basri & Browning 2009). Jackson & Jeffries (2013) have shown that the generally small amplitude of I-band light curves of the low-mass NGC 2516 members is quite consistent with $\beta \simeq 0.5$ if the spots are small and scattered over a large portion of the stellar surface.

The required spot coverage could be (much) lower if the inflated radii were also partly (or mostly) explained by the inhibition of convection due to a globally pervasive magnetic field (Macdonald & Mullan 2013; Feiden & Chaboyer 2012b, 2013). A relatively simple way to test the relative merits of the starspots versus globally inhibited convection scenarios is to compare the location of active stars and inactive field stars in various colour-magnitude diagrams (CMDs). Stauffer et al. (2003) pointed out that K-dwarfs in the Pleiades are nearly 0.5 mag sub-luminous compared to a MS isochrone in the M_V vs $(B-V)_0$ CMD and also significantly bluer (or sub-luminous) compared to much less active members of the older Praesepe cluster. However, in the M_V vs $(V-K)_0$ CMD the Pleiades members appear redder (or more luminous). How does this compare with the anticipated effects of magnetic inhibition of convection and/or starspots? Expansion driven by magnetic inhibition of convection would lead to a uniformly lower surface temperature (at a given luminosity) and should exclusively redden highly active stars relative to magnetically inactive stars in *both* CMDs. The effect of starspots depends on the spot temperature ratio. For darker starspots (with a temperature ratio $\leqslant 0.8$), the V-band flux density from the spotted area is a relatively small fraction (10 to 20 per cent) of the flux density from the unspotted photosphere. In this case the effect of starspots will be to shift magnetically active stars blueward in the M_V vs $(B-V)_0$ CMD. The extent of reddening, if any, in the M_V vs $(V-K)_0$ plane is less easy to predict since the spotted area would still make a significant contribution to the K-band flux.

Figure 10 shows CMDs for our sample of fast rotating stars in NGC 2516 and the Pleiades compared to empirical colour-magnitude relations for magnetically inactive MS stars from BM12, corrected to the metallicity and mean age of the clusters. Results are transformed from the radius-luminosity relations of BM12 to the colour-magnitude plane using their $(B-V)_0$ and

$(V-K)_0$ colour-temperature relations and the bolometric corrections in Fig. 8. Also shown in Fig. 10 are the predicted effects of:

- Magnetic inhibition of convection producing a uniform reduction in surface temperature. Curves are shown for a 10 percent increase in radius for MS stars and 30 per cent increase for PMS stars.
- A simplified, two temperature, model of a spotted star with 50 per cent coverage of starspots, assuming a uniform spot temperature ratio of 0.7 between the spotted and unspotted photosphere, giving β=0.40. Bolometric corrections for the spotted areas, which are outside the range of the colour-temperature relations of BM12, are taken from the BT-Settl model atmospheres (Allard et al. 2003).

Results in the M_V vs $(B-V)_0$ plane support the interpretation of Stauffer et al. (2003), that stars in the Pleiades are blue shifted relative to older, less magnetically active, stars because of significant spot coverage, though the blueward shift of the Pleiades stars is less than produced by a spot model with $\beta = 0.4$. However a model solely invoking global inhibition of convection to explain radius inflation appears to be ruled out by the observations. Results in the M_V vs $(V-K)_0$ are less clear cut. The model of a spotted star (with spot temperature ratio of 0.7) predicts a small blueing of active *MS stars* relative to inactive MS stars, whereas active MS stars in the Pleiades actually show a slight reddening. However, for the PMS regime at lower luminosities, and with more radius inflation, the two models make drastically different predictions. The low-mass PMS stars in NGC 2516 lie close to the empirical magnetically inactive locus and this is in reasonabe agreement with the prediction of the $\beta = 0.4$ spot model. However to explain a $\geqslant 30$ per cent radius inflation seen in these stars using global magnetic inhibition requires much lower surface temperatures at a given luminosity and results in a predicted locus that is *much* redder than observed. This either points to (unknown) problems in the indirect methods used for determing the radii of these low-mass PMS stars or indicates that global suppression of convection cannot be the sole cause of radius inflation and favours the starspot model.

It should be stressed that the modelled effects of starspots on the CMDs are qualitative in nature being based on a simple two temperature description of a spotted star. The real situation is likely to be more complex with spots and associated plages producing a range of surface temperatures.

6 SUMMARY

We have used a simple polytropic model to investigate the effect of dark starspots on the evolution and structure of magnetically active PMS stars. This model has been combined with an equivalent treatment of spotted main sequence stars by Spruit & Weiss (1986) to predict the level of radius inflation experienced by spotted stars as a function of their luminosity and spot coverage. The model has been compared with radii determined for magnetically active low-mass PMS stars in NGC 2516, for higher mass stars on or near the ZAMS in the Pleiades and NGC 2516, and for the tidally locked low-mass components of older eclipsing binary systems. Our results and conclusions can be summarised as follows:

(i) Starspots inflate the radii of PMS stars and slow their descent along Hayashi tracks. Radii are increased over unspotted stars of the same luminosity and age by a factor of $(1-\beta)^{-N}$, where β is the fractional coverage of dark spots and $N \simeq 0.45 \pm 0.05$. The temperature of unspotted regions of the photosphere is almost unchanged.

(ii) For a given β, the effect of starspots on PMS stellar radii is ~ 2 times greater than that predicted by Spruit & Weiss (1986) for main sequence stars of similar mass and luminosity, where $N \sim 0.2$–0.3 (see Fig. 4).

(iii) We find that highly magnetically active K- and M-dwarfs in the young Pleiades and NCG 2516 clusters and the tidally-locked binary low-mass components show a significant radius inflation relative to an empirical locus defined by inactive MS field stars; the mean increase in radius, at a given luminosity, ranges from 13 ± 3 per cent for MS K-dwarfs to 40 ± 4 per cent for the lower luminosity PMS M-dwarfs which are still on their Hayashi tracks.

(iv) The observed radius inflation could be caused by magnetic inhibition of convection or a high coverage of dark starspots or some combination of the two. If starspots are the sole cause of radius inflation, this requires a high coverage ($0.35 < \beta < 0.51$) of dark starspots.

(v) When compared to inactive main sequence stars, the loci of the highly active and inflated cluster stars in $(B-V)/V$ and $(V-K)/V$ colour-magnitude diagrams are more consistent with a high filling factor of dark starspots than an overall reduction of temperature caused by the suppression of convection. This evidence is strongest for the lowest mass PMS stars, where observed $V-K$ colours are far too blue to be explained by a globally reduced temperature if radii are inflated by 30–40 per cent.

ACKNOWLEDGEMENTS

RJJ wishes to thank the UK Science and Technology Facilities Council for finacial support.

REFERENCES

Alexander D. R., Ferguson J. W., 1994, Astrophys. J. , 437, 879
Allard F., Guillot T., Ludwig H., Hauschildt P. H., Schweitzer A., Alexander D. R., Ferguson J. W., 2003, in E. Martín ed., Brown Dwarfs Vol. 211 of IAU Symposium, Model Atmospheres and Spectra: The Role of Dust. pp 325–+
An D., Terndrup D. M., Pinsonneault M. H., 2007, ApJ, 671, 1640
Baraffe I., Chabrier G., Allard F., Hauschildt P. H., 1998, A&A, 337, 403
Boyajian T. S., McAlister H. A., van Belle G., 2012, Astrophys. J. , 746, 101
Boyajian T. S., von Braun K., van Belle G., 2012, Astrophys. J. , 757, 112
Carpenter J. M., 2001, AJ, 121, 2851
Chabrier G., Gallardo J., Baraffe I., 2007, A&A, 472, L17
Collier-Cameron A., Unruh Y. C., 1994, MNRAS, 269, 814
Cutri, R. M. et al. 2003, Technical report, Explanatory supplement to the 2MASS All Sky data release. http://www.ipac.caltech.edu/2mass/
Donati J.-F., Semel M., Carter B. D., Rees D. E., Collier Cameron A., 1997, MNRAS, 291, 658
Dotter A., 2008, ApJ, 687, L21
Eaton J. A., Hall D. S., 1979, Astrophys. J. , 227, 907
Feiden G. A., Chaboyer B., 2012, Astrophys. J. , 761, 30
Feiden G. A., Chaboyer B., 2013a, ArXiv e-prints 1309.7668
Feiden G. A., Chaboyer B., 2013b, Astrophys. J. , 779, 183
Hall D. S., 1972, Publ. astr. Soc. Pacif. , 84, 323
Hartman J. D., Bakos G. Á., Kovács G., Noyes R. W., 2010, MNRAS, 408, 475

Hayashi C., H ̄oshi R., Sugimoto D., 1962, Progress of Theoretical Physics Supplement, 22, 1
Herbst W., Mundt R., 2005, Astrophys. J. , 633, 967
Irwin J., Bouvier J., 2009, in E. E. Mamajek, D. R. Soderblom, & R. F. G. Wyse ed., IAU Symposium Vol. 258 of IAU Symposium, The rotational evolution of low-mass stars. pp 363–374
Jackson R. J., Jeffries R. D., 2010a, MNRAS, 402, 1380
Jackson R. J., Jeffries R. D., 2010b, MNRAS, 407, 465
Jackson R. J., Jeffries R. D., 2012, MNRAS, 423, 2966
Jackson R. J., Jeffries R. D., 2013, MNRAS, 431, 1883
Jackson R. J., Jeffries R. D., Maxted P. F. L., 2009, MNRAS, 399, L89
Jeffries R. D., 2007, MNRAS, 376, 1109
Jeffries R. D., Jackson R. J., Briggs K. R., Evans P. A., Pye J. P., 2011, MNRAS, 411, 2099
Johns-Krull C. M., Valenti J. A., 1996, in R. Pallavicini & A. K. Dupree ed., Cool Stars, Stellar Systems, and the Sun Vol. 109 of Astronomical Society of the Pacific Conference Series, Detection of strong magnetic fields on M dwarfs. pp 609–+
Krause F., Raedler K., 1980, Mean-field magnetohydrodynamics and dynamo theory. Pergamon Press, Oxford
Leggett S. K., 1992, Astrophys. J. Suppl. , 82, 351
López-Morales M., 2007, Astrophys. J. , 660, 732
MacDonald J., Mullan D. J., 2013, Astrophys. J. , 765, 126
Marcy G. W., 1982, Publ. astr. Soc. Pacif. , 94, 989
Meynet G., Mermilliod J.-C., Maeder A., 1993, A&AS, 98, 477
Morales J. C., Ribas I., Jordi C., Torres G., Gallardo J., Guinan E. F., Charbonneau D., Wolf M., Latham D. W., Anglada-Escudé G., Bradstreet D. H., Everett M. E., O'Donovan F. T., Mandushev G., Mathieu R. D., 2009, Astrophys. J. , 691, 1400
Mullan D. J., MacDonald J., 2001, Astrophys. J. , 559, 353
Noyes R. W., Weiss N. O., Vaughan A. H., 1984, Astrophys. J. , 287, 769
O'Neal D., 2006, Astrophys. J. , 645, 659
O'Neal D., Neff J. E., Saar S. H., 1998, Astrophys. J. , 507, 919
O'Neal D., Neff J. E., Saar S. H., Cuntz M., 2004, Astron. J. , 128, 1802
Pinsonneault M. H., Stauffer J., Soderblom D. R., King J. R., Hanson R. B., 1998, ApJ, 504, 170
Pizzolato N., Maggio A., Micela G., Sciortino S., Ventura P., 2003, A&A, 397, 147
Prialnik D., 2000, An Introduction to the Theory of Stellar Structure and Evolution. Cambridge University Press
Reiners A., Basri G., Browning M., 2009, Astrophys. J. , 692, 538
Reinhold T., Reiners A., Basri G., 2013, A&A, 560, A4
Rieke G. H., Lebofsky M. J., 1985, ApJ, 288, 618
Rozyczka M., Pietrukowicz P., Kaluzny J., Pych W., Angeloni R., Dékány I., 2013, MNRAS, 429, 1840
Semel M., 1989, A&A, 225, 456
Siess L., Dufour E., Forestini M., 2000, A&A, 358, 593
Soderblom D. R., Laskar T., Valenti J. A., Stauffer J. R., Rebull L. M., 2009, Astron. J. , 138, 1292
Spruit H. C., 1982, A&A, 108, 348
Spruit H. C., Weiss A., 1986, A&A, 166, 167
Stauffer J. R., Jones B. F., Backman D., Hartmann L. W., Barrado y Navascués D., Pinsonneault M. H., Terndrup D. M., Muench A. A., 2003, Astron. J. , 126, 833
Stauffer J. R., Schultz G., Kirkpatrick J. D., 1998, ApJ, 499, L199+
Strassmeier K. G., 2002, Astronomische Nachrichten, 323, 309
Terndrup D. M., Pinsonneault M., Jeffries R. D., Ford A., Stauffer J. R., Sills A., 2002, Astrophys. J. , 576, 950
Torres G., 2013, Astronomische Nachrichten, 334, 4
Torres G., Andersen J., Giménez A., 2010, A&ARv, 18, 67
van Leeuwen F., 2007, A&A, 474, 653

This paper has been typeset from a TEX/ LATEX file prepared by the author.